Published in "Supramolecular Chemistry 26(2): 125–137, 2014"
which should be cited to refer to this work.

Influence of linear and branched perfluoroalkylated side chains on the π–π stacking behaviour of hexa-peri-hexabenzocoronene and thermotropic properties

Bassam Alameddine[a]*, Olivier Frédéric Aebischer[b], Benoît Heinrich[c], Daniel Guillon[c], Bertrand Donnio[c]* and Titus A. Jenny[d]*

[a]*Department of Mathematics and Natural Sciences, Gulf University for Science and Technology, Hawally 32093, Kuwait;* [b]*BASF Pharma (Evionnaz) SA, G-ENP/OD, Route du Simplon 1, CH-1902 Evionnaz, Valais, Switzerland;* [c]*Institut de Physique et Chimie des Matériaux de Strasbourg (IPCMS), UMR 7504 (CNRS-Université de Strasbourg), 23 rue du Loess, BP43, 67034 Strasbourg cedex 2, France;* [d]*Department of Chemistry, University of Fribourg, Chemin du Musée 9, CH-1700 Fribourg, Switzerland*

The thermotropic properties and self-assembly of two different series of hexa-peri-hexabenzocoronenes (HBC) bearing either linear or branched perfluoroalkylated side chains, each with a wide range of alkyl spacer and perfluorinated tail lengths, have been studied. Correlations between thermogravimetric analysis, differential scanning calorimetry, polarised optical microscopy and small-angle X-ray scattering experiments revealed, as expected, that the transition temperatures and phase stability are influenced by the determining roles of the aliphatic spacer length and odd/even nature, as well as the size and structure (linear vs. bifurcation) of the perfluorinated sections. Most of the investigated HBC derivatives showed a single-column hexagonal columnar phase, where the columns are structured by a double segregation process between HBC aromatic cores and aliphatic spacers, on the one hand, and between aliphatic spacers and fluorinated tails, on the other hand. For the derivatives with long linear spacers, cores of untilted or quasi-untilted HBC stacks are surrounded by a cylindrical aliphatic envelope segregated from the fluorinated periphery, whereas for those with shorter linear spacers, the same structure is kept, except that the aliphatic envelope deviates from cylindricality and causes a symmetry break to rectangular envelope for the first term of the series. Of the four HBC with branched spacers, two are amorphous, whereas a columnar phase is maintained for the other two derivatives, but with tilted HBC stacks. Consequently, the evolution of the polymorphism in the series could be correlated with the variation of both interface areas.

Keywords: liquid crystals; self-assembly; supramolecular columns; polycondensed aromatic hydrocarbons; hexabenzocoronene; SAXS

Introduction

Self-assembly of organic and inorganic molecules through non-covalent, reversible bonding provides a versatile bottom-up approach to construct supramolecular architectures with self-healing properties (*1*). Hydrogen bonding (*2*), metal coordination (*3*) and π–π stacking (*4*) are the three main types of non-covalent bonding whose discrete or combined deployment (*5*) provides customised supramolecules with newly different chemical and physical properties than the single elementary constitutive building blocks.

Large discotic polyaromatic hydrocarbons (PAHs) having two-, three- or sixfold rotational symmetry (*6*) exhibit strong π interactions which induce their self-assembly into columnar structures (*7*). The relatively high charge carrier mobilities of these latter assemblies (*8*) made them potential candidates in many applied fields, especially as organic electronic materials (*9*).

Hexa-peri-hexabenzocoronene (HBC) (R = H, Chart 1) is the most prominent polyaromatic hydrocarbon due to its sixfold symmetry and versatile synthesis (*10*). Electron microscopy characterisation of ultra-thin layers of this compound on metallic surfaces revealed perfectly aligned columns showing little translation (*11*). When decorated with long aliphatic side chains, HBC derivatives become soluble in common organic solvents and show liquid crystalline behaviour over a wide temperature range (*10*, *12*, *13*). However, their self-assembly in the solid state affords closely packed columnar arrays with high intercolumnar interactions caused by the superior degree of crystallisation and packing order of the aliphatic side chains (*14*).

The remarkable impact of ring fluorination (*15*) and chain fluorination (*16–18*), in particular, on both molecular self-organisation and physicochemical properties, has been known for many years and is largely exploited for the elaboration of new materials targeted towards various practical applications. In this respect, the integration of semi-fluorinated chains within liquid crystalline materials has proven to be an interesting

*Corresponding authors. Email: titus.jenny@unifr.ch

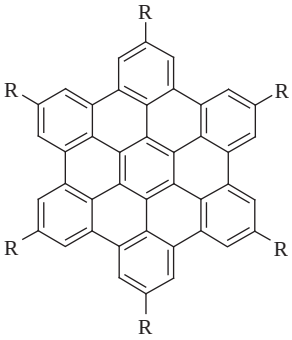

	linear				branched		
	R = $(CH_2)_n(CF_2)_mF$				R = $(CH_2)_nCH[(CH_2)_{n'}(CF_2)_mF]_2$		
	m = 4	m = 6	m = 8	m = 10		m = 4	m = 6
n = 2		**2a**	**3a***				
n = 3		**2b**	**3b**		n,n' = 3,1	**5a**	**5b***
n = 4	**1a**	**2c***	**3c***	**4a**	n,n' = 3,2		**5c**
n = 5		**2d**	**3d**		n,n' = 5,2		**5d**
n = 6		**2e***	**3e**				
n = 8	**1b**	**2f**	**3f**				

Chart 1. List of the investigated perfluoroalkylated hexabenzocoronene derivatives (HBC–$(R_{n,(n',)m})_6$). *These compounds were already reported in references 22 and 23.

strategy to modify and control phase separation from micro- to nano-scales, and to greatly enhance mesophase stability in classical mesogens (*15–17*) as well as in non-classical mesogenic materials (*16–20*).

We have previously reported the synthesis of a number of HBC derivatives bearing different perfluoroalkylated side chains, with linear (HBC–$[(CH_2)_n(CF_2)_mF]_6$) (Chart 1, series **1**–**4**) and branched topologies (HBC–$\{(CH_2)_nCH[(CH_2)_{n'},(CF_2)_mF]_2\}_6$) (Chart 1, series **5**), all showing a relatively good solubility in common organic solvents (*21*). Preliminary characterisation results of a few of these derivatives (Chart 1, compounds **2c**, **2e**, **3a**, **3c** and **5b**) (*22*, *23*), in the solid state (small-angle X-ray scattering, SAXS; cryo-SEM) and in solution (UV–vis absorption), have shown that these chains, composed of an inner aliphatic spacer and an outer perfluorinated segment, bestowed the HBC core with better self-assembly and higher thermal stability than their aliphatic analogues (*10*, *12*, *13*).

We observed that the number of methylene groups in the spacers (n) and the length of the fluorinated part (m), e.g. the ratio n/m, and particularly the aliphatic envelope significantly influence the packing order of the supramolecular systems. In this report, we show a comprehensive study of the thermal and self-organising behaviour of 19 perfluoroalkylated hexabenzocoronenes (including 5 derivatives previously reported) (*22*, *23*) investigated in details by thermogravimetric analysis (TGA), differential scanning calorimetry (DSC), polarising optical microscopy (POM), dilatometry and SAXS experiments.

Results and discussion

Thermal behaviour of the HBC derivatives bearing semi-fluorinated segments

The decomposition onset of the HBC derivatives, determined by TGA with a heating rate of 10°C·min^{-1} in air, occurred systematically before clearance between 205 and 275°C (Table 1 and Supporting Information, available online) depending on many factors: (i) the nature of the chains, e.g. linear as in series **1**–**4** or branched as in series **5**, (ii) total length ($n + m$) and (iii) aliphatic-to-fluorinated chain length ratio $r = n/(n + m)$. This prevented the determination of their isotropic liquid

Table 1. Phase sequences, decomposition temperature and ratio $r = n/(n + m)$ for all HBC–$(R_{n,m})_6$ and HBC–$(R_{n,(n',)m})_6$ compounds.

Acronym HBC–$(R_{n,(n',)m})_6$	Product	Transition temperatures (°C) and enthalpies (J g^{-1})[a]	Ratio $r = n/(n + m)$
HBC–$(R_{4,4})_6$	**1a**	Cr_1 109 (–)[b] Cr_2 145 (5.8) Cr_3 161 (1.4) Col_h ~210 dec.	0.5
HBC–$(R_{8,4})_6$	**1b**	I_{Col} ~210 dec.	0.67
HBC–$(R_{2,6})_6$	**2a**	Disordered solid phase 163 (0.3) Col_h ~275 dec.	0.25
HBC–$(R_{3,6})_6$	**2b**	Cr_1 93 (1.0) Cr_2 137 (0.8) Cr_3 167 (0.1) Col_h ~255 dec.	0.33
HBC–$(R_{4,6})_6$	**2c**	Cr_1 102 (1.0) Cr_2 156 (3.0) Cr_3 194 (6.2) Col_h ~235 dec.	0.4
HBC–$(R_{5,6})_6$	**2d**	Cr 120 (4.2) Col_h ~210 dec.	0.45
HBC–$(R_{6,6})_6$	**2e**	Cr_1 86 (4.6) Cr_2 109 (10.0) Col_h ~205 dec.	0.5
HBC–$(R_{8,6})_6$	**2f**	I_{Col} ~210 dec.	0.57
HBC–$(R_{2,8})_6$	**3a**	Cr_1 122 (1.1) Cr_2 138 (30.0) Cr_3 180 (6.2) Col_{hr} ~270 dec.	0.2
HBC–$(R_{3,8})_6$	**3b**	Cr 131 (3.5) Col_h ~250 dec.	0.27
HBC–$(R_{4,8})_6$	**3c**	Cr_1 82 (4.35) Cr_2 120 (42.1) Col_h ~240 dec.	0.33
HBC–$(R_{5,8})_6$	**3d**	Cr 115 (4.5) Col_h ~215 dec.	0.38
HBC–$(R_{6,8})_6$	**3e**	Cr1 77 (0.6) Cr2 96 (1.4) Cr3 115 (0.3) Col_h ~205 dec.	0.43
HBC–$(R_{8,8})_6$	**3f**	Cr1 97 (2.4) Cr2 113 (0.1) Col_h ~215 dec.	0.5
HBC–$(R_{4,10})_6$	**4a**	I_{Col} ~235 dec.	0.28
HBC–$(R_{3,1,4})_6$	**5a**	Col_h ~250 dec.	0.43
HBC–$(R_{3,1,6})_6$	**5b**	Amorphous solid phase ~275 dec.	0.33
HBC–$(R_{3,2,6})_6$	**5c**	Amorphous solid phase ~215 dec.	0.4
HBC–$(R_{5,2,6})_6$	**5d**	Col_h ~230 dec.	0.45

[a] Transition temperatures are given as the onset, obtained from the first DSC heating run (2°C/min), enthalpy of transition (J g^{-1}). Cri, crystalline phases; Colh, hexagonal columnar phase; Colr, rectangular mesophase with pseudo-hexagonal symmetry; ICol, isotropic liquid with long-range HBC stacks but with no orientation correlations; dec., decomposition temperature.
[b] Transition determined by XRD and not by DSC. The decomposition temperature is given at 2.5% weight loss from TGA measurements (Supplementary Information, available online).

transition temperatures and to obtain characteristic optical textures by POM. SAXS revealed that all mesomorphic HBC derivatives bearing linear chains (**1**–**4**) exhibit only one liquid crystalline phase, namely a 'single-column' hexagonal columnar phase (Col_h), occurring after several crystal-to-crystal phase transitions or, in the case of **2a** (n,m = 2,6), a Col_r mesophase directly from a disordered, almost amorphous solid phase. As for the branched derivatives (**5**), two of them show liquid crystalline properties at room temperature (Col_h), while the other two are amorphous solids.

The general tendency of the thermal behaviour consists in a melting transition temperature decrease with an increase in the length of the alkyl spacer (n), particularly obvious for compounds of the series HBC–$(R_{n,8})_6$ (Figure 1). This is expected since aliphatic chains are more flexible and, hence, melt at lower temperatures than the stiffer fluorinated chains (e.g. PE-HD melts at ~130°C and PTFE at ~330°C): the aliphatic spacers, thus, logically cause the early collapse of the crystalline structure. Beyond this general trend, there are some minor deviations among the medium variation in the HBC–$(R_{n,6})_6$ series and larger deviations in the HBC–$(R_{n,4})_6$ series. These deviations could be attributed to the discrepancy between the melting temperatures of the compounds bearing an even or odd number of methylene group spacers, the curve joining transition temperatures of the odd terms lying below the one joining the even terms. This result was not expected, but is classical in smectic systems (*24*) and can be easily explained by the influence of the orientation of the fluorinated chains with respect to the columnar core interface. Thus, the fluorinated chains are nearly orthogonal with respect to the columnar core in the absence of spacers or with even-numbered methylene groups (considering an all-trans alkyl chain conformation in the crystalline phase). In contrast, the orientation axis of the fluorinated chain is closer to a tangent with respect to the column when odd-numbered methylene units are present. Consequently, the supramolecular columns are better packed with even-numbered methylene spacers as compared with the more disordered odd-numbered methylene spacers. This corroborates with the more stable crystalline structure of HBC derivatives bearing the former

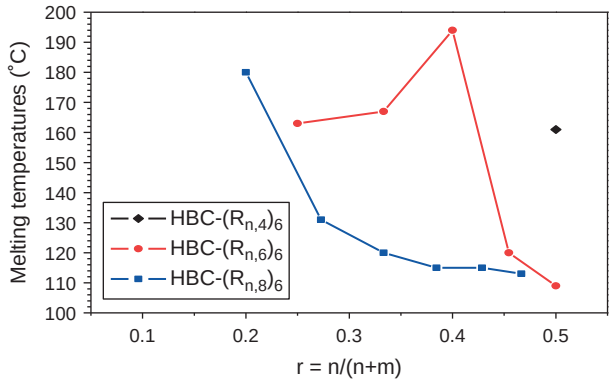

Figure 1. (Colour online) Variation of the melting temperatures into the Col_h phase for the HBC derivatives as a function of the ratio $r = n/(n + m)$.

chains as it can be deduced from their superior enthalpies of transition.

Unfortunately, the range of the fluorinated chain length variation is not large enough to properly separate its influence from the one of the alkyl spacer, but a general trend can be deduced. Thus, at low ratios (i.e. for long spacers), the general tendency corresponds to an increase in the melting temperature with increasing ratio. This can be understood as a shift of the melting temperature towards PTFE when the content of fluorinated chains increases. This variation might be extrapolated to higher chain ratios, but here the influence of the spacer becomes predominant, masking the influence of the fluorinated chain.

None of the branched derivatives were obtained in crystalline form, but are either amorphous or room temperature liquid crystalline materials, dictated by the alkyl-fluorinated ratio, i.e. governed by the ratio $r > 0.4$. Thus, by maintaining the fluorinated chain length constant at $m = 6$, the HBC derivative with the longest alkyl spacer (HBC–$R_{(5,2,6)6}$, **5d**) shows a liquid crystalline nature while those with the shorter alkyl groups (HBC–$R_{(3,1,6)6}$, **5b** and HBC–$R_{(3,2,6)6}$, **5c**) are amorphous. This is more likely an indication of the overcrowding at the periphery of the π-stacked columns, which impedes the segregation of the bulky fluorinated tails from the spacers and HBC in separated domains required to initiate organised structures. Logically, the lengthening of the spacer places the fluorinated tails away from each other and relaxes the steric constraints hindering the development of sharp interfaces. In contrast, the shortening of the fluorinated tails should not change the steric constraints and the diffuse interfaces between both types of chains. In this case, the reappearance of the organised structures probably follows the predominance of the segregation process between alkyl chains and HBC.

Small-angle X-ray diffraction analysis and mesomorphic self-assembly in Col_h

The liquid crystalline nature and symmetry of the supramolecular organisations formed by most fluorinated HBC derivatives were unambiguously confirmed by SAXS. Typically, diffraction patterns, recorded in the temperature range of the mesophase thermal stability, revealed up to six sharp, small-angle reflections, in the ratio $1{:}\sqrt{3}{:}\sqrt{4}{:}\sqrt{7}{:}\sqrt{12}{:}\sqrt{13}$, indicative of the long-range ordered two-dimensional (2D) hexagonal lattice of cylindrical columns with *p6mm* symmetry (N°17) (*25*), as commonly encountered with discotic mesogens (*26*). A wide-angled broad scattering halo was observed, occurring from lateral distances between molten semi-fluorinated alkyl chains, with a maximum located between 5.3 and 4.6 Å, depending on the respective contributions of the molten aliphatic and fluorinated chains: usually for molten aliphatic chains (h_H), the maximum should be located at 4.5 Å and for the fluorinated chains (h_F) at around 5.5 Å (h_H and h_F are visualised with arrows on the diffractograms, see representative examples of series 2 in Figure 2 and the whole set in Supporting Information, available online). An additional reflection which, depending on the compound, is either diffuse or sharp at about 3.6 Å (h_0), was also systematically present, occurring from the mean distance between neighbouring cores in the columnar stacks; this reflection corresponding to h_0 is no longer detected in the branched derivatives (vide infra).

Occasionally, an additional weak diffusion at mid-angle could be detected for some compounds, when not hidden by other neighbouring signals, corresponding to a distance of ca. 7.0–7.5 Å (i.e. $2h_0$), indicating an alternated stacking of the HBC cores (vide infra). Thus, all derivatives show the classical 'single-column' hexagonal columnar phase, Col_h, with the unique exception of HBC–$(R_{2,8})_6$ (**3a**). Patterns of this compound (*22*) contain an additional sharp reflection in the small-angle region, which reveals the doubling of the hexagonal lattice into a rectangular lattice with a pseudo-hexagonal symmetry: in such type of Col_r phase (*27*), the rectangular lattice parameter ratio is the one corresponding to the hexagonal case ($a/b = 3^{0.5}$), but because of the location of the columns in the lattice, or because of the organisation within the columns, there is no centring translation and the symmetry is reduced to the *p2gg* planar group (N°8) (*25*). Quite unexpectedly, as evidenced by the presence of broad small-angle scattering signals instead of sharp peaks (cf. Supporting Information, available online), three HBC derivatives bearing linear perfluoroalkylated chains do not show liquid crystalline properties, namely those with the largest aliphatic-to-fluorinated chain ratio *r*, defined as $r = n/(n + m)$ (i.e. $r = 0.67$ for HBC–$(R_{8,4})_6$, **1b** and $r = 0.57$ for HBC–$(R_{8,6})_6$, **2f**) or the one with the longest fluorinated tail ($m = 10$, $r = 0.28$, i.e. HBC–$(R_{4,10})_6$, **4a**). This lack of mesomorphism was further confirmed by the absence of birefringence during POM observations, excluding therefore the occurrence of a nematic columnar phase, N_{Col}. Actually, the phase change in the series essentially affects the small-angle region of the patterns and the large-angle scattering h_0 subsisting in the amorphous state. Consequently, the HBC piling is preserved and the small-angle scattering just consists in a reminiscence of the 2D lattice involving a few correlated HBC piles. This degree of residual positional ordering is unconventionally high in an amorphous phase, even comparable to that of the N_{Col} phase. A comprehensive analogy can be drawn with the Col_h to N_{Col} phase transition caused by the addition of hydrocarbons to discotic systems with a neat alkylated periphery (*28*): the expansion of the aliphatic continuum between the columns then leads to the loss of the long-range correlated positions. In these mixtures, the positional order is,

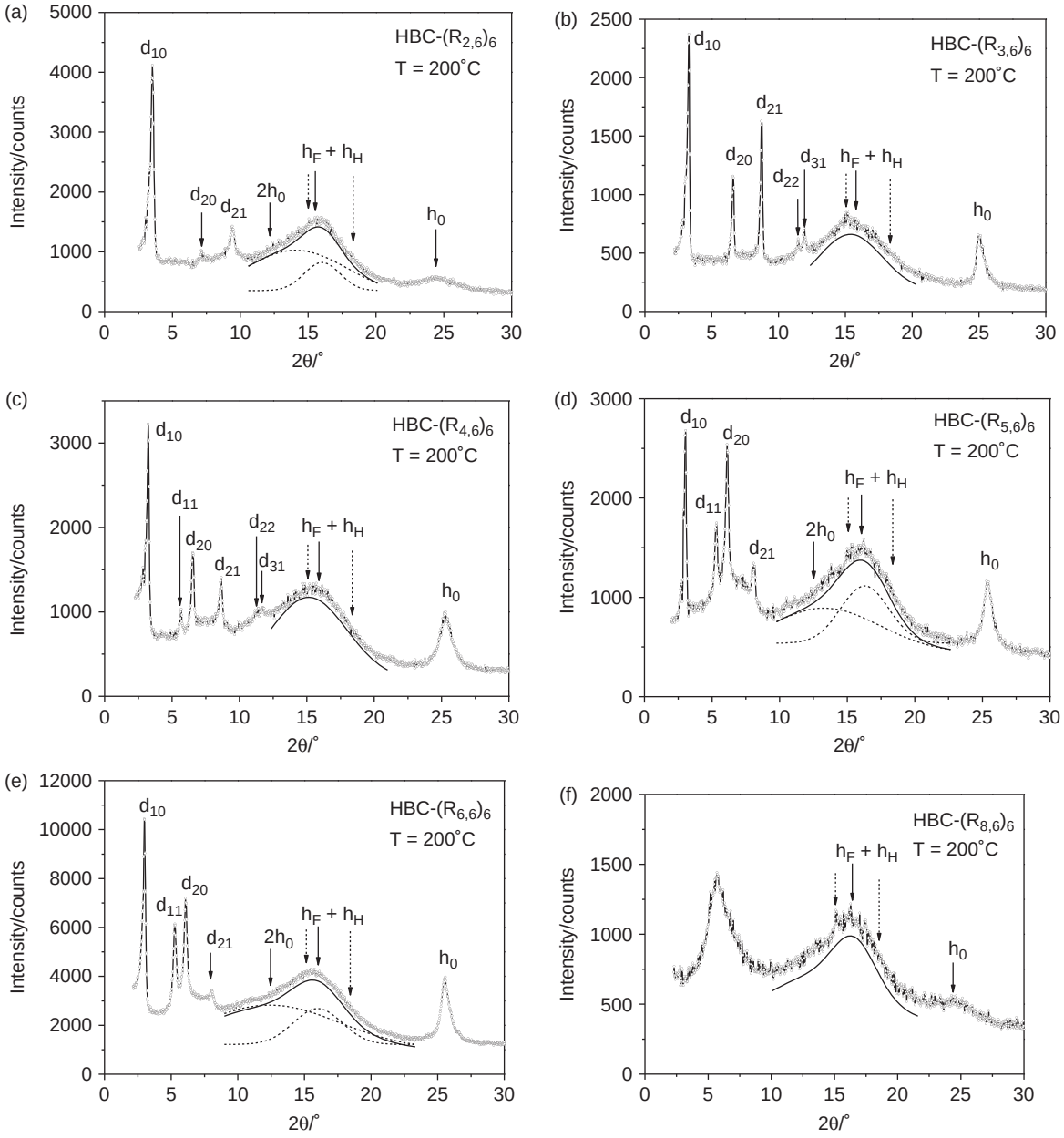

Figure 2. (a) HBC–$(R_{2,6})_6$, **2a**; (b) HBC–$(R_{3,6})_6$, **2b**; (c) HBC–$(Rf_{4,6})_6$, **2c**(*23*); (d) HBC–$(R_{5,6})_6$, **2d**; (e) HBC–$(R_{6,6})_6$, **2e** (*22*); (f) HBC–$(R_{8,6})_6$, **2f**. Dashed arrows: theoretical values of the average lateral distances between molten F-segment, h_F and H-segments, h_H; solid arrow: theoretical value of the average lateral distances between molten semi-fluorinated chains, $h_F + h_H$, as a function of the volume fraction of the respective segments (the detailed calculations are given in the Supplementary Information, available online).

however, intimately connected to the preservation of the orientational long-range order characterising the nematic phase and the wide-angle region is in particular no more decomposable into separate scatterings after crossing to the isotropic liquid phase. On the contrary, the present HBC derivatives show a columnar short-range order persisting even in the isotropic phase, with no preferential orientation of the columns along one direction as in N_{Col} (thus, this reminiscent self-organised assembly will be thereafter referred to as I_{Col}). This reminiscence is obviously a consequence of the strong segregation between both incompatible liquid chains separating the HBC piles. On the opposite side of the series, the compound showing the pseudo-hexagonal phase, Col_r-$p2gg$, also possesses the largest discrepancy r^* ($r* = 1-r$) between fluorinated and aliphatic sections (i.e. HBC–$(R_{2,8})_6$, **3a**, $r* = 0.8$). Outside these rough limits set by the parameter r, the melting temperature

towards the Col_h phase for all the other derivatives is essentially tuned by the respective lengths of both the aliphatic and fluorinated chains (Figure 1).

In conclusion, SAXS experiments clearly confirm the assignment of the mesophases as Col_h in most cases, with the notable exception of the presence of a Col_r phase (HBC–$(R_{2,8})_6$, **3a**). The detailed composition of the X-ray patterns measured at 200°C for all liquid crystalline HBC derivatives is presented in Supporting Information, available online. At this temperature, all members of the series are in the columnar hexagonal mesophase, facilitating the comparison of the structural parameters and also of the evolution of the patterns regarding the number and respective intensities of higher order reflections. In mesophases, the liquid-like lateral packing between equivalent molecular fragments merges them into volumes of constant electronic density, and the juxtaposition of the segregated volumes containing antagonistic fragments generates the long-range ordered average structure, consisting of columns separated by a continuous medium in a 2D arrangement. Higher order reflections provide then information on the sharpness and regularity of interfaces and on the deviation from cylindricality of the column shape. Moreover, reflection intensities and the lattice geometry could discriminate between the different segregation processes leading to the columnar structure. Thus, in pure aliphatic-HBC systems (*10*, *12*, *13*), the structure unequivocally associates HBC columns and aliphatic periphery, but here the additional segregation between fluorinated and aliphatic segments could lead to different structures involving a columnar lattice: (i) the stratification of columns constituted by HBC and spacers surrounded by the fluorinated continuum; (ii) the split of the fluorinated periphery into additional columns alternating with HBC, as observed in dendritic materials (*29*); (iii) the split into sublayers alternating with rows of columns forming lamello-columnar phases (*30*). The latter case is unlikely as the alternation of lamellae and rows in a particular direction of the lattice should break the hexagonal symmetry, which occurs for a single derivative (see discussion below). The models based on intermingled homogeneous columns or on a unique type of stratified columns are both compatible with the observed symmetry, but would lead to different lattice areas and interface areas per chain segment. Moreover, these models suppose a different distribution of the HBC, aliphatic and fluorinated domains, and therefore a different electronic density distribution in the lattice.

The difficulty in the calculation of the electronic densities lies in estimating correctly the partial volumes of the three segregating parts. Thus, the partial volumes of both types of liquid chains are known from reference dilatometric measurements on alkanes and semi-perfluoroalkyl alkanes (the variation of the volumes as a function of temperature are given in Supporting Information, available online), leading to electronic densities at 200°C of 0.26 $Å^{-3}$ (7.4×10^{10} cm^{-2} after the renormalisation with the Thomson's electron radius) for the aliphatic spacers and ranging from 0.41 to 0.50 $Å^{-3}$ (11.5 to 14×10^{10} cm^{-2}) for the fluorinated segments, whose partial volume is less familiar, in particular regarding the contribution of CF_3 end groups. Dilatometric data on HBC fragments are unfortunately not available, but the partial volume is roughly estimated to 650 $Å^3$ from single crystal structures (*31*), corresponding to a electronic density of 0.41 $Å^{-3}$ (11.5×10^{10} cm^{-2}). Despite uncertainties, these calculations show that the electronic density contrast between HBC and fluorinated domains is small, whereas the contrast between these latter parts and the aliphatic domains is huge. Intermingled and stratified columns, therefore, lead to a very different electronic density distribution in the lattice. The former model comes down to the classical columnar core–shell organisation, with the high electronic density nodes associated with HBC and fluorinated columns. Both cases of undifferentiated columns in a single-column lattice and of individualised columns defining a super-lattice with several columns may then occur (*16*, *18*, *20*, *29*). In the stratified column model, the fluorinated parts form a continuous periphery whose electronic density is similar to the HBC cores, whereas the aliphatic intermediate envelope constitutes a valley of electronic density. This then leads to a single-column lattice resembling to the one of pure aliphatic mesogen systems, except that the objects contrasting with the periphery now come down to tubes (i.e. the aliphatic shell) instead of solid cylinders (the mesogen cores).

The vanishing of the contrast between core and periphery fatally drops the intensity of the fundamental row periodicity and raises the intensity of higher order reflections in phase with the aliphatic shell size. Indeed, in all patterns, the (10) reflection is of comparable intensity or even weaker than other reflections (see Figure 2 and Supporting Information, available online), whereas in pure aliphatic (*13*) or in intermingled (e.g. Ref. *29*) systems, its intensity generally dominates the pattern by several orders of magnitude). Models with a core-to-periphery main contrast as the latter systems are thus definitively ruled out here, whereas stratification with the main contrast between the envelope and the rest of the lattice is in agreement with the appearance of patterns. Going on with this model, the precise modulation of the reflection intensities is finely depending on the location of the inner and outer envelope boundaries and thus of the volume fractions of the three domains, which is consistent with the progressive intensity ratio changes observed in the series. For instance, the first term ($n = 2$) of the HBC–$(R_{n,6})_6$ series (Figure 2) gives rise to a slightly raised (21) reflection, though far less intense than (10). Both (21) and (20) reflections grow for the next term ($n = 3$) to about the half and the third of (10) reflection, respectively. Further spacer lengthening ($n = 4$–6) leads to a progressive intensity decrease of

(21) and to a further growing of (20), relayed by the growing of (11), the ultimate term of the series ($n = 8$) being not any more columnar. To resume, the modulation maximum regularly shifts along the series, from slightly beyond (21), up to in-between (20) and (11) reflections. A very similar modulation maximum variation is found for HBC–$(R_{n,8})_6$ series in a spacer length range logically shifted by about one unit ($n = 3$–8), as this shift compensates the larger fluorinated volume fraction and leaves the location of the aliphatic envelope in the lattice roughly unchanged in reduced coordinates (cf. Supporting Information, available online).

The aliphatic volume fraction (f_H) is smaller for the very first term of the HBC–$(R_{n,8})_6$ series ($n = 2$) than for any other HBC derivative, and this is likely related to the observed doubling of the 'single-column' lattice into a primitive rectangular lattice, revealing a non-cylindrical average column shape. All other derivatives show a single-column hexagonal lattice consistent with the average cylindrical column shape, but deviations from this shape might occur all the same and not be long range correlated. These shape irregularities would then preserve the *p6 mm* symmetry, but influence the reflection intensity modulation. Conversely, the degree of agreement between the experimental intensity modulation and the one expected for cylindrical boundaries reveals to what extent the structuration between chains shifts from the perfect segregated one, realised with cylindrical interfaces of minimum area (see Figure 3(a)). Unfortunately, parameterising cylinder sizes is a tricky step because of uncertainty on partial volumes and on the real electronic density ratios. Moreover, the comparison with experience is also delicate, because of the large Debye–Waller factor leading to the rapid damping of higher order reflections, in relation with the limited sharpness of interfaces in the liquid crystalline state. Aware of these limitations, the experimental intensity ratios are all the same faced to square structure factor ratios from models with both extreme segregation patterns: perfectly cylindrical and sharp interfaces, or continuum of chains without interfaces, respectively. These calculations were performed with parameters deduced from volume fractions by assuming perfect identity of electronic densities of HBC and fluorinated chains, which reduces the former model to a lattice of hollow columns (i.e. tubes) and the reference model to the classical solid column case (see Figure 3(b),(c)).

In consistency with experience, the tube model predicts considerably lowered (10) reflections and amplified higher order reflections, the amplitude of the modulation expanding with the spacer length, i.e. with the wall thickness and the average diameter of tubes (see Figure 4). Moreover, the position of the modulation maximum and, therefore, the intensity ratios between higher order reflections logically shift with the average diameter, but in a smaller scale than experimentally observed.

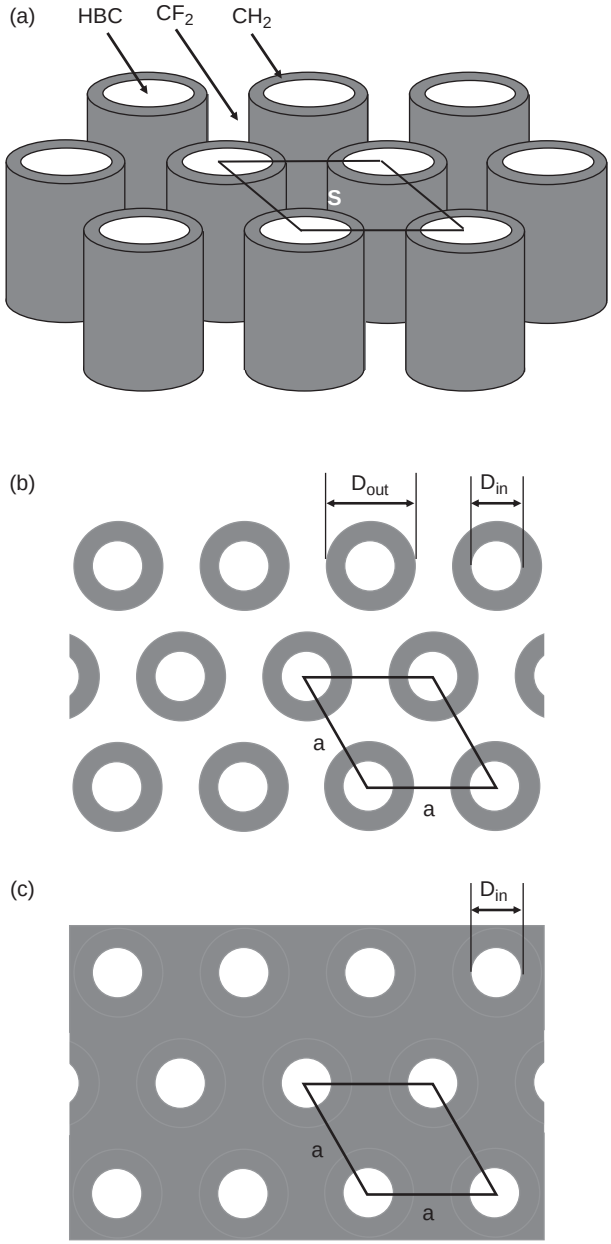

Figure 3. (a) Model of the hexagonal lattice in the Col_h phase for a perfect double segregation of hexabenzocoronene (HBC), aliphatic spacers (CH_2) and fluorinated tails (CF_2) into straight infinite concentric columns with cylindrical interfaces (perspective view). (b) Model lattice in top view: as electronic densities of HBC and CF_2 are similar, the lattice reduces to a packing of hollow columns (i.e. tubes) of CH_2, whose inner and outer diameters (D_{in} and D_{out}) are determined by the lattice size (lattice parameter a and area S) and the respective volume fractions of the three parts. (c) Reference model without segregation of CH_2 and CF_2, reducing to a classical packing of solid columns of HBC in an undifferentiated continuum of CH_2 and CF_2, the column diameter being, thus, the same as D_{in} of the tube model. Individual electronic density charts for both tube and solid columns models were then generated for each HBC–$(R_{n,m})_6$ derivative showing the Col_h phase. The ratios of square structure factors of the 4 first reflections visible in most patterns were then deduced from these charts and faced to reflection intensity ratios in patterns (Figure 4).

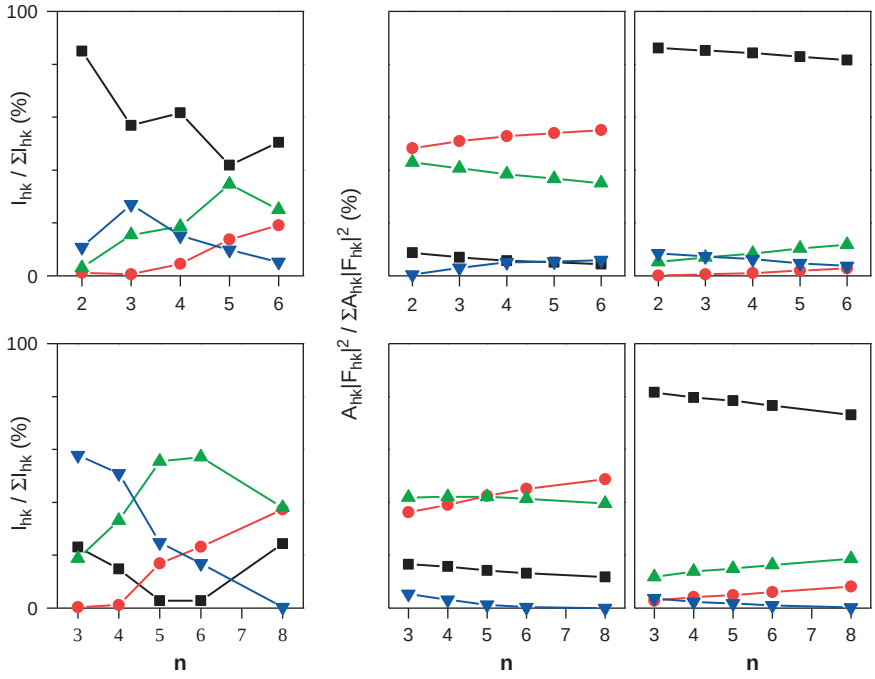

Figure 4. (Colour online) Intensity ratios (IR_{hk}) of reflections (10) (squares, -■-), (11) (discs, -●-), (20) (up−triangles, -▲-) and (21) (down−triangles, -▼-), according $IR_{hk} = I_{hk}/(I_{10} + I_{11} + I_{20} + I_{21})$ (ordinates from 0% to 100%), in the HBC−$(R_{n,6})_6$ (top) and HBC−$(R_{n,8})_6$ (bottom) series. Left: raw IR_{hk} determined from patterns. Middle and right: ratios between products of square structure factors and reflection multiplicity ($AFFR_{hk}$), as calculated for a perfect segregation of HBC and both types of chain into concentric cylindrical columns (middle) and for the absence of any segregation between chains (right), according to models shown in Figure 3. Theoretical intensity ratios would be deduced from $AFFR_{hk}$ by the multiplication with a Debye−Waller Factor depending on the sharpness of interfaces. This factor decreases at an unknown rate along the reflection series and $AFFR_{hk}$ therefore overestimate the theoretical IRhk of higher order reflections, which must be considered when facing with experimental IR_{hk}.

In particular, the structure factor ratios move closer to experimental intensity ratios for long spacer homologues, but fail to reproduce the amplification of the (21) reflection at small spacer lengths. This large discrepancy between model prediction and experience at small aliphatic volume fractions is partly due to the high weight of the neglected contribution of the scattering between HBC and fluorinated parts, in connection with the uncertainties on partial volumes and electronic densities. However, at small aliphatic volume fractions, the segregation from the fluorinated periphery is also less efficient, explaining that intensity ratios of the first term ($n = 2$) of the HBC−$(R_{n,6})_6$ series are even better reproduced by the solid column model than the tube model. From a molecular point of view, this large deviation from tube model implies that the spacers stretch in certain directions and intercalate with refolding tails. This process would then go up to the loss of the average cylindrical shape of the columns and to the symmetry break to *p*2*gg* observed for the derivative with smallest aliphatic volume fraction, i.e. the first term ($n = 2$) of the HBC−$(R_{n,8})_6$ series.

In these highly symmetrical mesophases, the information from intensity ratios is not sufficient to really discriminate between different types of interface shapes and prevent us to discuss more complicated models. Nevertheless, as any deviation from cylindricality ends in the expansion of interface areas; this feature is likely imposed by the molecular packing near one or both interfaces and might be explained by simple geometrical considerations.

Thus, the average distances between aliphatic chains ($h_H \approx 0.9763 \cdot \sigma_H^{0.5} = 4.8$ Å, where $\sigma_H \approx 24.1$ Å^2 is the cross section of a molten chain at 200°C) (*32*) and fluorinated chains ($h_F \approx 0.9763 \cdot \sigma_F^{0.5} = 5.9$ Å, with $\sigma_F \approx 36.0$ Å^2 at 200°C) (*29*) largely exceeds the thickness of the aromatic cores (stacking distance $h_0 \approx 3.6$ Å, directly determined from X-ray patterns). To accommodate these discrepancies, the molecules are likely stacked in a staggered fashion, i.e. with a rotation of approximately 30° (as sometime evidenced by the occurrence of a signal at $2h_0$), where the chains of one HBC fill the empty space between the chains of the two flanked first neighbouring HBCs, as demonstrated in a previous molecular dynamics study (*23*) (Supporting Information, available online). The intermolecular repeating distance along the columnar axis *h* can be deduced by dividing the theoretical molecular volume V_{mol} by the lattice area *S* ($S = 1/2; |a^2 3^{0.5}$) (*26*, *27*, *33*) (Table SI section). This periodicity is a statistical

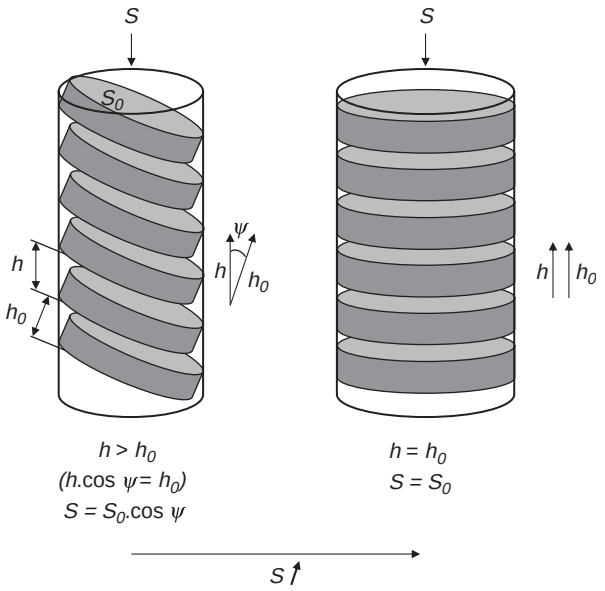

Figure 5. Representation of two modes of stacking of discs within columns and the different parameters h, h_0, S and S_0 (obtained from X-ray diffraction and dilatometry) allowing for their discrimination. Ψ is the angle between the columnar axis and the molecular disc normal (*36*).

average distance in the long-range correlated columnar domains and needs to be compared to h_0, which characterises the local packing of HBC cores. Indeed, the difference ($\Delta h = h - h_0$) gives an indication on the distortion of the self-aggregated strands forming the columns. A small value of Δh indicates that the molecules are preferentially stacked perpendicularly and are not tilted with respect to the columnar axis. For larger Δh values, the individual molecules start to get more tilted with respect to each other as illustrated in Figure 5. It should be mentioned that Δh can also be negative in the case of undulating columns (*34*, *35*).

In the case of the HBC derivatives with linear chains, h and h_0 deviate by $< 10\%$ from each other, for the longest spacers, and by $< 15\%$, for the shortest spacers (Figure 6 (a)). These small deviations are significant, despite the errors included in the molecular volume calculations, but their magnitude is compatible with the fluctuations of the disc orientations inside the columns. Consequently, the columns can be considered as composed of untilted or quasi-untilted discs. Further details of the packing could be brought about with more accuracy, thanks to the fortuitous coincidence of the variations of S versus total chain length for the HBC–$(R_{n,6})_6$ and the HBC–$(R_{n,8})_6$ series (Figure 6(b)). From the common parabolic fit equation and from the molecular volume equations (involving the gap between the volumes of CF_2 and of CH_2 groups, i.e. 47.5 and 30.6 Å^3 at 200°C, respectively), the mean variation of h with total chain length could be superposed to experimental points, making an accurate comparison possible between series and between terms of series (Figure 6(a)). Concerning the influence of the fluorinated tail length, both the single compound with C_4F_9 tails and the series with C_8F_{17} tails show slightly but significantly higher h values than the series with the intermediate C_6F_{13} tails. Within both series, there is a clear odd–even effect: S lies systematically above and h below the medium variations for the derivatives with an odd number of CH_2 per spacer (and vice versa for the derivatives with an even number of CH_2 per spacer).

The concentric cylindrical column model as represented in Figure 3 corresponds to the structure minimising interfaces between both antagonistic liquids and represents, moreover, the apparent average organisation compatible with the phase symmetry and geometrical parameters in all cases except HBC–$(R_{2,8})_6$ (see above). Nevertheless, the analysis of reflection intensities showed that the real packing deviates from this average apparent packing, for which sterical constrains near interfaces might

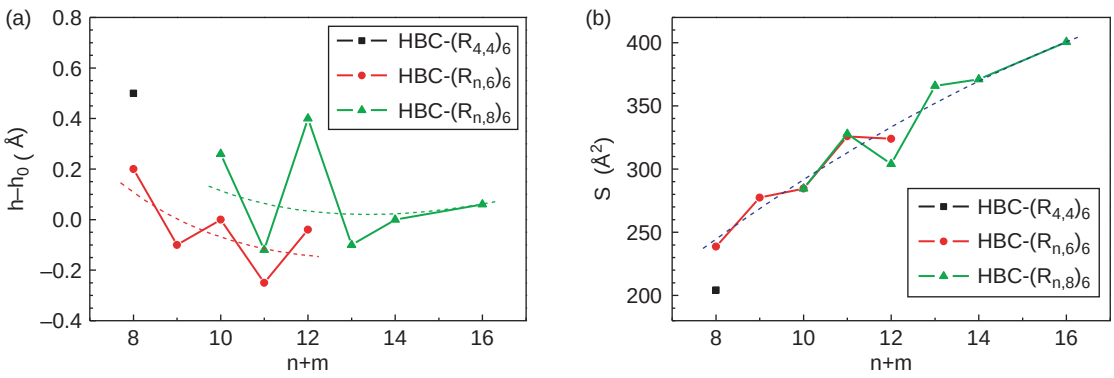

Figure 6. (Colour online) Variations versus total chain–length (total number of carbons in the aliphatic spacer and in the fluorinated tail) at 200 °C of (a) the difference between the repeating distance along the columns, h, and the mean distance between neighboring cores, h_0, and (b) the columnar section. Dashed lines in (a) are the mean variations for both series. The dashed line in (b) is the common parabolic fit for the HBC–$(R_{n,6})_6$ and the HBC–$(R_{n,8})_6$ series.

be responsible. Indeed, deviations from cylindricality would fatally occur in the case of a discrepancy between the natural cross sections of molten chains σ ($\sigma_H \approx 24$ Å^2 and $\Sigma_F \approx 36$ Å^2, for both types of chains at 200°C) and the cylinder portion area covered by these chains Σ ($\Sigma_H = (\pi/6) \times D_{in} \times h$ and $\Sigma_F = (\pi/6) \times D_{out} \times h$, D_{in} and D_{out} being the inner and outer diameters of the tube containing the aliphatic spacers, as deduced from the lattice area and from the calculated volume fractions of the three molecular parts; Σ_H and Σ_F refer to the nature of the chains beyond the interface, i.e. the aliphatic spacers and the fluorinated tails, respectively). So, the case $\Sigma < \sigma$ excludes the cylindrical sharp interfaces since the area allocated to a single chain is not sufficient; conversely, it demonstrates that the real area is then enlarged by a deformation process from a sharp cylinder, e.g. oval cross sections or pinching zones along the columnar strands (*37*). The case $\Sigma >> \sigma$ is possible since the molten chains may fold and tilt, but this is not satisfactory for the segregation. Real systems may compromise this mechanism and a competitive one consisting in cylinder undulations (*34*).

The interface areas per chain at the HBC–spacer interface Σ_H and at the spacer–tail interface Σ_F are plotted in Figure 7(a),(b) and compared to the cross sections σ_H and σ_F, respectively. At the inner interface, Σ_H exceeds σ_H by 15–25% throughout the series, implying that the aliphatic spacers are slightly folded. At the outer interface, Σ_F is close to σ_F for the first term of the series and increases then logically by lengthening the spacers. Interface areas are thus large enough for cylindrical columns in the case of the long spacers, for which this shape is in agreement with patterns, and also in the case of the short spacers, for which the shape obviously deviates from cylindricality. The deviation at small spacer lengths is therefore not forced by the bulky fluorinated chains but rather accommodates the loose crowding of the spacers, which would then group on opposite sides of the HBC columns. The aliphatic envelope is then mechanically thinned in the plane perpendicular to the grouping, which for sufficiently short spacer leads to the splitting of the envelope into opposite halves (Figure 8). The respective positions and orientations between half envelopes of neighbouring columns would then explain the lattice doubling and the symmetry reduction to *p*2*gg* for HBC–$(R_{2,8})_6$. For slightly larger aliphatic fractions, the elongation of the aliphatic envelope stops below the splitting and the symmetry break, but could modify the electronic density distribution in the hexagonal lattice in a way, explaining the discrepancies between experience and predictions of the tube model. For substantially larger aliphatic fractions, the envelope is necessarily continuous and the average shape then approximates a cylinder to minimise interfaces between incompatible liquids. However, the discrepancy between Σ_F and cross sections continuously increases with the aliphatic fraction and needs to be compensated by the chains refolding, introducing shape irregularities, such as bumps, hollows, bents and so on. These irregularities logically induce fluctuations in the respective positions of HBC piles and finally lead to the loss of the long-range positional ordering above a certain Σ_F value, as experimentally observed for the ultimate terms of the series. Unlike columnar systems with a pure aliphatic periphery, the crossing to the amorphous phase is, here, primarily due to the expansion of the interface between both liquids instead of the disorder in the mesogen piling, and this is likely the reason for the persistence of marked h_0 and small-angle scatterings in the amorphous phase (Figure 8).

Beyond the evolution of the packing as a function of the spacer length and the fluorinated chain length, the most important parameter consists in the parity of the spacer length. Thus, the derivatives with odd spacers exhibit smaller areas per interfaces than the corresponding derivatives with even spacers. At first sight, this result is surprising since tails connected to even spacers are supposed to emerge rather radially and the tails connected to odd spacers more tangentially from the interface.

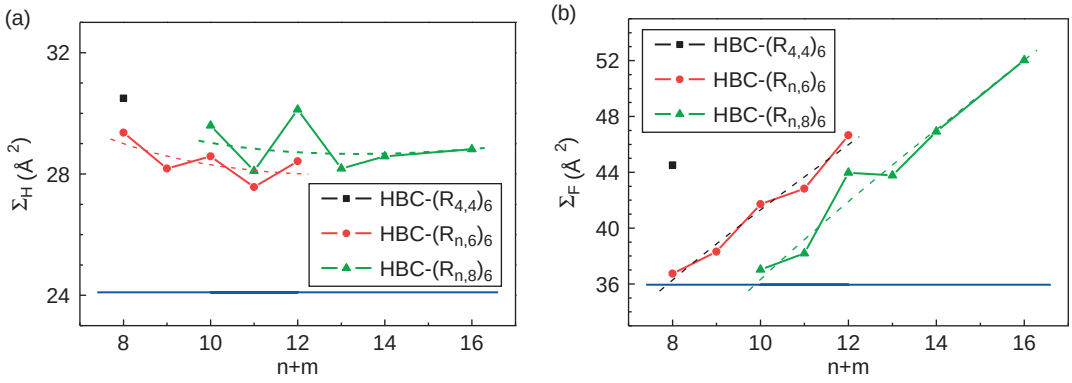

Figure 7. (Colour online) Variations versus the total chain–length at 200 °C of the areas per chain at both interfaces for the packing model in Figure 3. (a) interface between stacked cores and aliphatic envelope; (b) interface between aliphatic envelope and fluorinated continuum. The parallel lines to the abscissa axis represent the cross section of molten aliphatic chains and molten fluorinated chains.

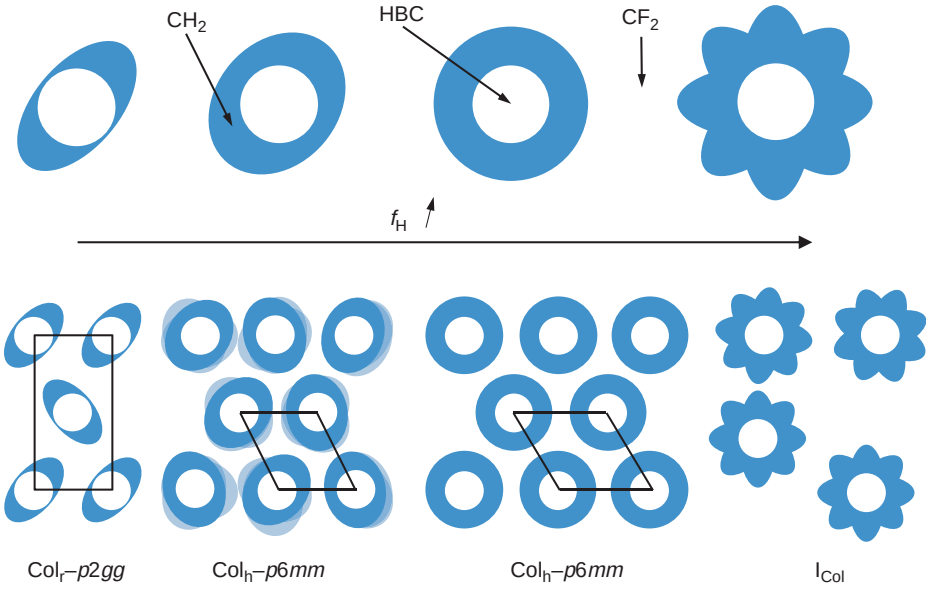

Figure 8. (Colour online) Schematic view of the evolution of the packing with the aliphatic volume fraction (f_H) in the HBC linear chain derivative series. (a) Two-columns Col_r-*p2gg* lattice with split aliphatic envelope for the first term of the series; (b, c) single-column Col_h-*p6 mm* lattice with elongated interface shape at small aliphatic fractions, becoming more cylindrical at larger fractions; (d) particular isotropic phase (I_{Col}) for the ultimate terms of the series, in which the columnar stacking is preserved, but the columns stay short range correlated, likely in relation with the irregular interface shape.

Logically, the projection of a single tail section onto the interface is then larger in the odd spacer case, in apparent inconsistency with experience. However, this discrepancy would be resolved with a lateral shift between the more tangentially emerging tails: the projected areas of neighbouring tails would then superpose, leading to a thicker interface zone and therefore to a reduced interface area. At this stage, this idea remains very speculative, and the influence of the spacer length parity should be more extensively investigated in comparative studies. Moreover, this would also highlight the odd–even effect evidenced in the variations of the transition temperatures (see above).

Beyond details, HBC derivatives with linear chains give rise to columnar organisations with columns made of untilted or quasi-untilted HBC stacks surrounded by an aliphatic envelope and a fluorinated periphery, those common interfaces tuning the polymorphism. Although for the linear chain derivatives the chain cross sections are always below the available interface area, relations are reversed in the derivatives with branched chains. Disappearance or changes of the mesophase properties might have been expected, but the HBC–$(R_{5,2,6})_6$ derivative turned out to exhibit a Col_h phase all the same. If the segregation between both types of liquids is maintained in this phase, the accommodation of interface areas needs to increase either h or the ratio Σ_F/h, which is respectively realised by elongating columns through tilts of HBC cores and by deforming the interface between chains. The first mechanism is obviously the one taking place, since h now exceeds h_0 by more than 60% (5.9 Å compared to 3.6 Å), while both distances were similar in the linear chain derivatives. Indeed, the elongation in HBC–$(R_{5,2,6})_6$ amounts to HBC cores tilted by 52° and to an average cylindrical interface area matching the cross section of tails ($\Sigma_F \approx 36$ Å$^2 \approx \sigma_F$). Fulfilling this area matching condition for both HBC–$(R_{n,n',6})_6$ derivatives with shorter chains would have required even larger elongations ($h \approx 7.0$ and 8.5 Å) and tilts (angles around 60° and 65°), but the mesophase is not preserved for these samples, which stay amorphous at all temperatures. In fact, large tilts are detrimental to an efficient segregation in stacks, in relation with the expanded interface towards the periphery, and also with the reduced number of mesogens interacting in perpendicular to their plane. These weakened interactions translate into the broadening and the blurring out of the h_0 scattering, and for large tilts into the complete vanishing of the scattering (*38*), and indeed this scattering is undetectable in the Col_h phase of HBC–$(R_{5,2,6})_6$ as in the amorphous phase of both homologue derivatives. Unlike the amorphous phase in the linear derivatives (see above), the one in the branched derivatives is therefore a classical isotropic phase, devoid of short-range correlated columnar order, as the loss of the mesophase is mainly caused by the disorder in the piling of mesogens here and in the respective positions of neighbouring stacks in the former case. Finally, the isolated derivative with branched chains was composed of short aliphatic spacers and short fluorinated tails, HBC–$(R_{3,1,4})_6$ also gives rise to a Col_h phase, but in this case the stacking of the mesogens

predominates the segregation in the periphery and imposes not so high elongation ($h \approx 4.6$ Å) and tilt (38°). The corresponding cylindrical interface area is only of 28 Å^2, i. e. comprised between σ_H and σ_F, showing conversely that the interface between both chains deviates substantially from a cylinder with sharp interfaces. Intuitively, the mechanism should be that the weaker segregation between short chains gives rise to a mixing zone compensating the smaller interface area imposed by the HBC stacks. But this hypothesis needs confirmation in a future more extensive work.

Conclusion

The observed supramolecular organisations have been comprehensively and efficiently described by the help of classical concepts, such as partial molecular volumes, and transverse cross sections of molecular segments applied at both interfaces generated by the specific triblock molecular architecture. Except the amorphous ultimate terms of the series, all HBC derivatives with linear chains show a columnar organisation with a double segregation process: one between HBC and aliphatic spacers and the other between this latter and the fluorinated tails. In the derivatives with long linear spacers, the 'single-column' lattice is always of hexagonal geometry, with columns constituted of a core of untilted or quasi-untilted HBC stacks and a cylindrical aliphatic envelope. The same structure is kept for the HBC derivatives with shorter linear spacers, except that the aliphatic envelope which deviates from cylindricality and finally leads to a break towards the rectangular *p2gg* symmetry for the first term of the series. Some of the HBC derivatives with branched chains still show a similar hexagonal columnar phase, but with tilted HBC stacks, the tilt angle being induced by the expansion of the interface between both types of chains due to branching. The other branched derivatives stay amorphous at all temperatures.

Supporting Information

Tables of indexation, phase parameters, X-ray diffraction patterns, electronic density charts, thermogravimetry curves, molecular dynamic simulation and cryo-SEM micrographs are available in Supporting Information.

References

(1) Lange, R.F.M.; Van Gurp, M.; Meijer, E.W. *J. Polym. Sci.* **1999**, *37*, 3657–3670.

(2) (a) Lehn, J.M. *Supramolecular Chemistry.* Wiley: New York, 1995;p. 281. ISBN: 978-3-527-29311-7; (b) Steed, J.W.; Atwood, J.L. *Supramolecular Chemistry*, 2nd ed.; Wiley: New York, 2009;p. 990. ISBN: 978-0470-51233-3; (c) Sijbesma, R.P.; Meijer, E.W. *Chem. Commun.* **2003**, 5–16; (d) Prins, L.J.; Reinhoudt, D.N.; Timmerman, P. *Angew. Chem. Int. Ed.* **2001**, *40*, 2382–2426; (e) Sherrington, D.C.; Taskinen, K.A. *Chem. Soc. Rev.* **2001**, *30*, 83–93.

(3) (a) Saalfrank, R.W.; Maid, H.; Scheurer, A. *Angew. Chem. Int. Ed.* **2008**, *47*, 8794–8824; (b) Ruben, M.; Rojo, J.; Romero-Salguero, F.J.; Uppadine, L.H.; Lehn, J.-M. *Angew. Chem. Int. Ed.* **2004**, *43*, 3644–3662; (c) Piguet, C.; Bernardinelli, G.; Hopfgartner, G. *Chem. Rev.* **1997**, *97*, 2005–2062; (d) Hosseini, M.W. *Acc. Chem. Res.* **2005**, *38*, 313–323; (e) Mamula, O.; Von Zelewsky, A. *Coord. Chem. Rev.* **2003**, *242*, 87–95 and references therein; (f) Swiegers, G.F.; Malefetse, T.J. *Chem. Rev.* **2000**, *100*, 3483–3538; (g) Michelsen, U.; Hunter, C.A. *Angew. Chem. Int. Ed.* **2000**, *39*, 764–767; (h) Gorman, C. *Adv. Mater.* **1998**, *10*, 295–309; (i) Sauvage, J.P.; Collin, J.P.; Chambron, J.C.; Guillerez, S.; Coudret, C.; Balzani, V.; Barigelletti, F.; Cola, L.D.; Flamigni, L. *Chem. Rev.* **1994**, *94*, 993–1019.

(4) (a) Nakano, T.; Yade, T. *J. Am. Chem. Soc.* **2003**, *125*, 15474–15484; (b) Gallivan, J.P.; Schuster, G.B. *J. Org. Chem.* **1995**, *60*, 2423–2429; (c) Engelkamp, H.; Middelbeek, S.; Nolte, R.J.M. *Science* **1995**, *284*, 785–788.

(5) (a) Brunsveld, L.; Lohmeijer, B.G.; Vekemans, J.A.; Meijer, E.W. *Chem. Commun.* **2000**, *23*, 2305–2306; (b) Lightfoot, M.; Mair, F.S.; Pritchard, R.G.; Warren, J.E. *Chem. Commun.* **1999**, *19*, 1945–1946; (c) Palmans, A.R.; Vekemans, J.A.; Havinga, E.E.; Meijer, E.W. *Angew. Chem. Int. Ed.* **1997**, *36*, 2648–2651.

(6) Doetz, F.; Brand, J.D.; Ito, S.; Gherghel, L.; Müllen, K. *J. Am. Chem. Soc.* **2000**, *122*, 7707–7717.

(7) (a) Yatabe, T.; Harbison, M.A.; Brand, J.D.; Wagner, M.; Müllen, K.; Samori, P.; Rabe, J.P. *J. Mater. Chem.* **2000**, *10*, 1519–1525; (b) Watson, M.D.; Fechtenchötter, A.; Müllen, K. *Chem. Rev.* **2001**, *101*, 1267–1300 and references therein; (c) Brunsveld, L.; Folmer, B.J.B.; Meijer, E.W.; Sijibesma, R.P. *Chem. Rev.* **2001**, *101*, 4071–4097; (d) Arikainen, E.O.; Boden, N.; Bushby, R.J.; Lozman, O.R.; Vinter, J.G.; Wood, A. *Angew. Chem. Int. Ed.* **2000**, *39*, 2333–2336.

(8) (a) Van de Craats, A.; Warman, J.M.; Müllen, K.; Geerts, Y.; Brand, J.D. *Adv. Mater.* **1998**, *10*, 36–38; (b) Adam, D.; Schuhmacher, P.; Simmerer, J.; Haeussling, L.; Siemensmeyer, K.; Etzbach, K.H.; Ringsdorf, H.; Haarer, D. *Nature* **1994**, *371*, 141–143.

(9) (a) Samori, P.; Severin, N.; Simpson, C.D.; Müllen, K.; Rabe, J.P. *J. Am. Chem. Soc.* **2002**, *124*, 9454–9457; (b) Kumar, S. *Chem. Soc. Rev.* **2006**, *35*, 83–109; (c) Laschat, S.; Baro, A.; Steinke, N.; Giesselmann, F.; Hägele, C.; Scalia, G.; Judele, R.; Kapatsina, E.; Sauer, S.; Schreivogel, A.; Tosoni, M. *Angew. Chem. Int. Ed.* **2007**, *46*, 4832–4887; (d) Sergeyev, S.; Pisula, W.; Geerts, Y.V. *Chem. Soc. Rev.* **2007**, *36*, 1902–1929; (e) Kumar, S. *Liq. Cryst.* **2009**, *36*, 607–638; (f) Pisula, W.; Zorn, M.; Chang, J.Y.; Müllen, K.; Zentel, R. *Macromol. Rapid Commun.* **2009**, *30*, 1179–1202.

(10) Ito, S.; Wehmeier, M.; Brand, J.D.; Kübel, C.; Epsch, R.; Rabe, J.P.; Müllen, K. *Chem. Eur. J.* **2000**, *6*, 4327–4342.

(11) Ruffieux, P.; Gröening, O.; Bielman, M.; Simpson, C.; Müllen, K.; Schlapbach, L.; Gröening, P. *Phy. Rev. B* **2002**, *66*, 073409/073401–073409/073404.

(12) (a) Kastler, M.; Pisula, W.; Wasserfallen, D.; Pakula, T.; Muellen, K. *J. Am. Chem. Soc.* **2005**, *127*, 4286–4296; (b) Lee, M.; Kim, J.-W.; Peleshanko, S.; Larson, K.; Yoo, Y.-S.; Vaknin, D.; Markutsya, S.; Tsukruk, V.V. *J. Am. Chem. Soc.* **2002**, *124*, 9121–9128; (c) Fechtenchoetter, A.; Tchebotareva, N.; Watson, K.; Muellen, K. *Tetrahedron* **2001**, *57*, 3769–3783; (d) Thünemann, A.F.; Kubowizc, S.K.; Burger, C.; Watson, M.D.; Tchebotareva, N.; Müllen, K. *J. Am. Chem. Soc.* **2003**, *125*, 352–356.

(13) Herwig, P.; Kayser, C.W.; Müllen, K.; Spiess, H.W. *Adv. Mater.* **1996**, *8*, 510–513.
(14) Stabel, A.; Herwig, P.; Müllen, K.; Rabe, J. *Angew. Chem. Int. Ed. Engl.* **1995**, *34*, 1609–1611.
(15) Hird, M. *Chem. Soc. Rev.* **2007**, *36*, 2070–2095.
(16) Tschierske, C. *Top. Curr. Chem.* **2012**, *318*, 1–108.
(17) Krafft, M.-P.; Riess, J.G. *Chem. Rev.* **2009**, *109*, 1714–1792.
(18) Tschierske, C. *Chem. Soc. Rev.* **2007**, *36*, 1930–1970.
(19) Rosen, B.M.; Wilson, C.J.; Wilson, D.A.; Peterca, M.; Imam, M.R.; Percec, V. *Chem. Rev.* **2009**, *109*, 6275–6540.
(20) Ungar, G.; Tschierske, C.; Abetz, V.; Holyst, R.; Bates, M. A.; Liu, F.; Prehm, M.; Kieffer, R.; Zeng, X.; Walker, M.; Glettner, B.; Zywocinski, A. *Adv. Funct. Mater.* **2011**, *27*, 1296–1323.
(21) (a) Aebischer, O.F.; Muñoz, D.T.; Tondo, P.; Débieux, J.-L.; Jenny, T.A. *Synthesis* **2010**, 1123–1140; (b) Aebischer, O.F.; Aebischer, A.; Tondo, P.; Alameddine, B.; Dadras, M.M.; Güdel, H.-U.; Jenny, T.A. *Chem. Commun.* **2006**, 4221–4223.
(22) Alameddine, B.; Aebischer, O.F.; Amrein, W.; Donnio, B.; Deschenaux, R.; Guillon, D.; Savary, C.; Scanu, D.; Scheidegger, O.; Jenny, T.A. *Chem. Mater.* **2005**, *17*, 4798–4807.
(23) Aebischer, O.F.; Aebischer, A.; Donnio, B.; Alameddine, B.; Dadras, M.; Güdel, H.-U.; Guillon, D.; Jenny, T.A. *J. Mater. Chem.* **2007**, *17*, 1262–1267.
(24) Watanabe, J.; Komura, H.; Niiori, T. *Liq. Cryst.* **1993**, *13*, 455–465.
(25) *International Tables for Crystallography*; 4th ed. Revised ed. Dordrecht/Boston/London, 1995; Vol. A Space-Group Symmetry.
(26) Levelut, A.-M. *J. Chim. Phys.* **1983**, *80*, 149–160.
(27) Morale, F.; Date, R.W.; Guillon, D.; Bruce, D.W.; Finn, R. L.; Wilson, C.; Blake, A.J.; Schröder, M.; Donnio, B. *Chem. Eur. J.* **2003**, *9*, 2484–2501.
(28) (a) Seghrouchni, R.; Skoulios, A. *J. Phys. II (France)* **1995**, *5*, 1385–1405; (b) Rusjan, M.; Donnio, B.; Heinrich, B.; Cukiernik, F.D.; Guillon, D. *Langmuir* **2002**, *18*, 10116–10121.
(29) Bury, I.; Heinrich, B.; Bourgogne, C.; Mehl, G.H.; Guillona, D.; Donnio, B. *New J. Chem.* **2012**, *36*, 452–468.
(30) Cardinaels, T.; Ramaekers, J.; Nockemann, P.; Driesen, K.; Van Hecke, K.; Van Meervelt, L.; Lei, S.; De Feyter, S.; Guillon, D.; Donnio, B.; Binnemans, K. *Chem. Mater.* **2008**, *20*, 1278–1291.
(31) Goddard, R.; Haenel, M.W.; Herndon, W.C.; Krueger, C.; Zander, M. *J. Am. Chem. Soc.* **1995**, *117*, 30–41.
(32) Marcos, J.; Giménez, R.; Serrano, J.-L.; Donnio, B.; Heinrich, B.; Guillon, D. *Chem. Eur. J.* **2001**, *7*, 1006–1013.
(33) Donnio, B.; Heinrich, B.; Allouchi, H.; Kain, J.; Diele, S.; Guillon, D.; Bruce, D.W. *J. Am. Chem. Soc.* **2004**, *126*, 15258–15268.
(34) Donnio, B.; Heinrich, B.; Gulik-Grzywicki, T.; Delacroix, H.; Guillon, D.; Bruce, D.W. *Chem. Mater.* **1997**, *9*, 2951–2965.
(35) Pucci, D.; Barberio, G.; Bellusci, A.; Crispini, A.; Donnio, B.; Giorgini, L.; Ghedini, M.; La Deda, M.; Ildyko Szerb, E. *Chem. Eur. J.* **2006**, *12*, 6738–6747.
(36) Aebischer, O.; Alameddine, B.; Jenny, T.A. *Chimia* **2008**, *62*, 967–972.
(37) (a) Sakya, S.P.; Seddon, J.M.; Templer, R.H.; Mirkin, R.J.; Tiddy, G.J.T. *Langmuir* **1997**, *13*, 3706–3714; (b) Chaia, Z.; Heinrich, B.; Cukiernik, F.; Guillon, D. *Mol. Cryst. Liq. Cryst.* **1999**, *330*, 151–158; (c) Mysliwiec, D.; Donnio, B.; Chmielewski, P.J.; Heinrich, B.; Stepien, M. *J. Am. Chem. Soc.* **2012**, *134*, 4822–4833.
(38) Weber, P.; Guillon, D.; Skoulios, A. *Liq. Cryst.* **1991**, *9*, 369–382.